Radiometric Comparison between GeoEye-1 and WorldView-2 Panchromatic and Multispectral Imagery

Manuel A. Aguilar, María del Mar Saldaña, Fernando J. Aguilar, Ismael Fernández

Polytechnic High School and Faculty of Experimental Sciences, Department of Engineering. University of Almería, Spain, belonging to the Agrifood Campus of International Excellence ceiA3 (http://www.ceia3.es/)

Article Information

Keywords:
GeoEye-1
WorldView-2
VHR satellite images
Radiometric characteristics
Digital values

Corresponding author:
Manuel A. Aguilar
Tel.:+34950015997
Fax.:+34950015491
e-mail: maguilar@ual.es
Address: Ctra. de Sacramento s/n. La Cañada de San Urbano, 04120 Almería, Spain.

Abstract

Nowadays the couple of commercial very high resolution (VHR) satellites more innovative and unexplored are GeoEye-1 and WorldView-2, launched in September 2008 and October 2009 respectively. GeoEye-1 is currently the commercial satellite with the highest geometric resolution for panchromatic (PAN) and multispectral (MS) imagery, i.e. 0.41 m GSD (Ground Sample Distance) at nadir for PAN imagery and 1.65 m GSD for MS images, including the four classic bands: blue, green, red and near infrared (B, G, R, Nir). On the other hand WorldView-2, with 0.46 m and 1.84 m nominal resolution at nadir in PAN and MS images respectively, presents improved multispectral characteristics, since it includes four newly added bands such as coastal (C), yellow (Y), red edge (Re) and near infrared-2 (Nir2).
The images from these sensors are often used to produce orthoimages, digital elevation models (DEMs), digital surface models (DSMs) and land-cover and land-use maps by means of remote sensing classification. In this way, the importance of the radiometric characteristics of the VHR imagery on the accuracy of these products has been already contrasted. In this work, the radiometric characteristics of several PAN and MS Geo images from GeoEye-1 have been compared over the same working area with another Ortho Ready Standard Level-2A (ORS2A) PAN and MS images from WorldView-2. Both Geo and ORS2A products are radiometrically corrected and projected to a plane with constant height having nearly the same processing level. However, the radiometric characteristic turned out to be very different.

1 Introduction

The launch of the first very high resolution (VHR) satellites, IKONOS in September 1999, with 1 m as the nominal ground sample distance (GSD) in panchromatic (PAN), and QuickBird in October 2001, with 0.61m as the nominal GSD, meant the beginning of a new age in remote sensing. In fact, with these VHR satellites, the old prediction from an article making predictions for the next century published in 1900 by the magazine Ladies Home Journal (cited by John Croft [1]) which said: “Flying machines will carry powerful telescopes that beam back to Earth photographs as distinct and large as if taken from across the street”, has come true, almost right on time.

Besides, many new VHR satellites, capable of capturing PAN imagery of the land surface with GSD of 1 m and even lower, such as EROS B1, Resurs DK-1, KOMPSAT-2, IRS Cartosat 2, WorldView-1, have been launched during 2006 and 2007, and they are offering to their customers very high resolution imagery of the Earth, with a revisit time very shortly.

Nowadays the couple of commercial very high resolution (VHR) satellites more innovative and unexplored are GeoEye-1 (GE1) and WorldView-2 (WV2), launched in September 2008 and October 2009 respectively. GE1 is currently the commercial satellite with the highest geometric resolution, i.e. 0.41 m GSD at nadir for PAN imagery and 1.65 m GSD for multispectral (MS) images, including the four classic bands: blue, green, red and near infrared (B, G, R, Nir). On the other hand, WV2, with 0.46 m and 1.84 m nominal resolution at nadir in PAN and MS images respectively, presents improved multispectral characteristics, since it includes two sets of MS bands (MS1 and MS2). The MS1 set contains the conventional MS bands (B, G, R, Nir), whereas the MS2 set consists of four newly added bands such as coastal (C), yellow (Y), red edge (Re) and near infrared-2 (Nir2). In a comparative analysis of two VHR sensors (IKONOS and WV2) for mapping urban tree species, Pu and Landry [2] achieved interesting results. In the last work, overall accuracy was increased by 16–18% using WV2 imagery compared to that using IKONOS imagery. Improved results with the WV2 sensor were attributed to improved spatial resolution (4 m to 2 m) and additional bands (coastal, yellow, red-edge and NIR2).

The PAN images from both sensors are often used to produce high accurate orthoimages [3], [4], [5], and [6] and digital elevation models (DEMs) or digital surface models (DSMs) [7] and [8]. On the other hand, the MS images are usually employed to generate land-cover and land-use maps by means of object-based image analysis (OBIA) classification. In this way, the importance of the radiometric characteristics of the images on the accuracy of these products has been already contrasted. For example, when an automated area based matching procedure is applied, radiometrically blurred images lead to bring more successful matching pairs but also resulted in more inaccurate matching points in the extracted DSMs [9] and [10]. Furthermore, the differences observed between the possible radiometric distribution and visual appearance of PAN and MS images from GE1 and WV2 VHR satellites could result in different classification accuracy [11].

Within the chain from image sensing to the final value-added product the quality of the images plays a crucial

role. Image quality is defined by several parameters, as the radiometric resolution and its accuracy, represented by the noise level, and the geometrical resolution and sharpness. These parameters are usually described by the Modulation Transfer Function (MTF) [12] and [13]. However, a new No-Reference assessment of image quality based on blur and noise has been proposed [13].

In this work, the radiometric characteristics based on Digital Numbers (DNs) of several PAN and MS Geo images from GE1 have been compared over the same working area with another Ortho Ready Standard Level-2A (ORS2A) PAN and MS images from WV2. Both Geo and ORS2A products are radiometrically corrected and projected to a plane with constant height having nearly the same processing level.

2 Study site

The study area comprises the heavily developed coastal fringe of Almería (Mediterranean Sea, Southern Spain), approximately 11 km long and 775 m wide. The working area is situated between the harbours of Garrucha and Villaricos (Fig. 1). It is centred on the WGS84 coordinates (easting and northing) of 605870 m and 4119869 m.

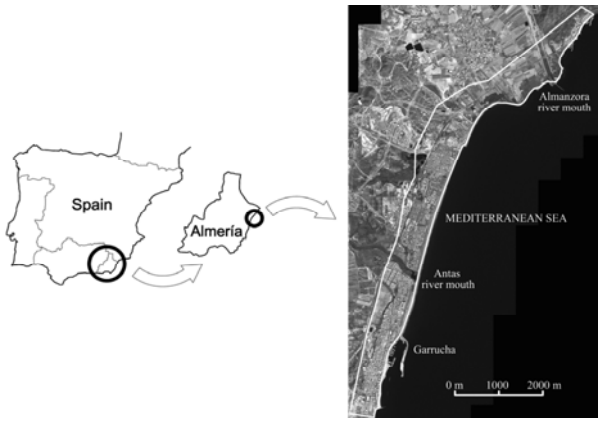

Fig. 1 Location of the study site.

3 WV2 Data

A map-projected WV2 ORS2A 8-bands PAN and MS (including MS1 and MS2) images, covering the whole working area, was acquired on July 19, 2011. Likewise, a WV2 stereo pair containing two PAN images was taken on August 18, 2011. The stereo pair was ordered in ORS2A format, covering the entire working area. Only one of the last aforementioned images belonging to the stereo pair, was also taken in MS. The WV2 images were shipped with a dynamic range of 11-bits and without any colour correction or contrast enhancement. The complete characteristics of the WV2 images are shown in Tab 1.

4 GE1 Data

Three bundle (PAN + MS) images from GE1 were also taken from 2010 to 2011 (Tab 2). The images were ordered with a dynamic range of 11-bits per pixel and without any adjustment (i.e. maintaining absolute radiometric accuracy and full dynamic range for scientific applications). Two of these images (GE12 and GE13) were composed a stereo pair. It is worth noting that the single images making up the GeoStereo pair product are identical to Geo product single images. All the images from GE1 and WV2 presented 0.5 m and 2 m GSD for PAN and MS mode respectively.

Image ID	WV21	WV22	WV23
Acquisition Date	19/7/2011	18/8/2011	18/8/2011
Product	ORS2A	ORS2A	ORS2A
Acquisition Time (GTM)	11:23	11:22	11:23
Cloud Cover	0%	0%	0%
Scan Direction	Forward	Forward	Reverse
Sun Azimuth	142.5°	152.3°	152.8°
Sun Elevation	70.5°	63.7°	63.8°
Collection Elevation	85.0°	67.6°	80.0°
Collection Azimuth	279.9°	4.7°	216.1°
Collected Col GSD (PAN)	0.47 m	0.50 m	0.47 m
Collected Row GSD (PAN)	0.46 m	0.54 m	0.48 m
Product Pixel Size (PAN)	0.5 m	0.5 m	0.5 m
Collected Col GSD (MS)	1.87 m	-	1.89 m
Collected Row GSD (MS)	1.86 m	-	1.90 m
Product Pixel Size (MS)	2 m	-	2 m
Bits per Pixel	11	11	11

Tab. 1 Characteristics of PAN and MS images from WV2.

Image ID	GE11	GE12	GE13
Acquisition Date	29/9/2010	27/8/2011	27/8/2011
Product	Geo	GeoStereo	GeoStereo
Acquisition Time (GTM)	11:01	10:55	10:56
Cloud Cover	0%	0%	0%
Scan Direction	Reverse	Reverse	Reverse
Sun Azimuth	159.3°	144.1°	144.4°
Sun Elevation	48.4°	58.3°	58.4°
Collection Elevation	69.4°	81.5 °	66.9°
Collection Azimuth	221.9°	40.4 °	183.6°
Collected Col GSD (PAN)	0.46 m	0.42 m	0.48 m
Collected Row GSD (PAN)	0.45 m	0.42m	0.44 m
Product Pixel Size (PAN)	0.5 m	0.5 m	0.5 m
Collected Col GSD (MS)	1.84 m	1.66 m	1.92 m
Collected Row GSD (MS)	1.80 m	1.65 m	1.76 m
Product Pixel Size (MS)	2 m	2 m	2 m
Bits per Pixel	11	11	11

Tab. 2 Characteristics of PAN and MS images from GE1 Geo and GeoStereo.

5 Radiometric Analysis Methodology

The radiometric characteristics of each VHR satellite image were studied in three different ways: (i) by means of the histograms of digital numbers (DNs), (ii) using visual inspection, and finally, (iii) computing blur and noise ratios for carried out an No-Reference image quality assessment according to Choi et al. [14].

5.1 Histograms of digital numbers

In this section, the histograms of DNs corresponding to the whole working area for each band from the original (non orthorectified) map-projected and 16-bits VHR MS and PAN images tested in this work are going to be computed and compared. In the case of the MS GE1 images, the conventional bands (i.e. R, G, B and Nir) will be computed, whereas for WV2, both MS1 and MS2 bands will be considered.

5.2 Visual inspection

After the histograms analysis described above, a visual inspection were carried out in order to compare subjective visual differences with the numerical values previously attained. This visual analysis was undertaken on PAN and MS images. For that the same square shaped area of 140 m (i.e. 19600 m^2) was used.

5.3 Image quality assessment

Assessment for image quality traditionally needs its original image as a reference. The conventional method for assessment like Mean Square Error (MSE) or Peak Signal to Noise Ratio (PSNR) is invalid when there is no reference. Choi et al. [14] proposed a new No-Reference assessment of image quality using both blur ratio (*Br*) and noise ratio (*Nr*), which gives high correlation with subjective Difference Mean Opinion Score (DMOS). Although image quality is affected by many features like hue, edge, noise, and contrast, Choi et al. [14] assumed that noise and blur were the most important factors on image quality degradation. The idea is to use these new ratios for describing the radiometric quality of the PAN and MS VHR satellite images, until now usually defined by MTF [12] and [13].

Both *Br* and *Nr* are measured by simple numeric operations on pixel's DN. We are going to describe the way for computing these ratios according to Choi et al. [14]. First of all and to establish the *Br*, two steps are needed: First is edge detection and second is blur decision. For the first stage, if the test image is denoted with *M* rows and *N* columns as $f(x,y)$, for $x \in [1,M]$ and $y \in [1,N]$, then the horizontal absolute difference value of a pixel is defined by:

$$D_h(x,y) = |f(x,y+1) - f(x,y-1)| \quad (1)$$

The mean value of the horizontal absolute difference value for every pixel in the image is calculated by:

$$D_{h-mean} = \frac{1}{M \times N} \sum_{x=1}^{M} \sum_{y=1}^{N} D_h(x,y) \quad (2)$$

In the case of the horizontal absolute difference value of a pixel (i.e. equation 1) is larger than the mean value (i.e. equation 2), the pixel becomes edge candidate $C_h(x,y)$. If the $C_h(x,y)$ of center pixel is bigger than horizontally adjacent pixels $\{C_h(x,y-1), C_h(x,y+1)\}$, the pixel is determined to be on the edge. The decision of edge pixel $E_h(x,y)$ is summarized as follows:

$$C_h(x,y) = \begin{cases} D_h(x,y) if\ D_h(x,y) > D_{h-mean} \\ 0 \quad Otherwise \end{cases} \quad (3)$$

$$E_h(x,y) = \begin{cases} 1\ if\ D_h(x,y-1) < C_h(x,y) > D_h(x,y+1) \\ 0 \quad Otherwise \end{cases} \quad (4)$$

Now, to make the decision about if a specific edge pixel is blurred or not, the horizontal blur ratio (BR_h) is computed following (5) and (6):

$$A_{h(x,y)} = \frac{1}{2} D_h(x,y) \quad (5)$$

$$BR_h(x,y) = \frac{|f(x,y) - A_h(x,y)|}{A_h(x,y)} \quad (6)$$

In the same way, the vertical blur ratio (BR_v) is also calculated. The larger value between BR_h and BR_v (*maxBR*) is selected for final decision, which is called inverse blurriness by Choi et al. [14].

$$B(x,y) = \begin{cases} 1\ if\ maxBR < Th \\ 0 \quad Otherwise \end{cases} \quad (7)$$

The equation (7) means the center pixel with inverse blurriness (or *maxBR*) under a threshold (*Th*) is considered as blurred. Note that *Th* was fixed at 0.1 as proposed Choi et al. [14]. Finally, the blur ratio (Br) to the edge is calculated by:

$$Br = \frac{Blur_{cnt}}{Edge_{cnt}} \quad (8)$$

Where $Blur_{cnt}$ is the count of blurred pixels and $Edge_{cnt}$ is the total number of edge pixels.

Regarding noise, Choi et al. [14] proposed to measure the noise out of the edge region. The edge detection can also be affected by noise. Hence, a pre-processing for noise filtering is needed prior to detecting the edge. Choi et al. [14] applied an average filter to the test image to remove the noise. The averaging filtered image $g(x,y)$ was generated by:

$$g(x,y) = \frac{1}{3x3} \left[\sum_{i=-1}^{1} \sum_{j=-1}^{1} f(x+i, y+i) \right] \quad (9)$$

We obtain the edge pixels on $f(x,y)$ in the similar way to blur measurement. D_h and $D_{h\text{-}mean}$ are computed as (1) and (2), as well as in vertical direction. In this way the noise candidate which is zero on edge region (N_{cand}), take the maximum value of ($D_h(x,y)$, $D_v(x,y)$) when $D_h(x,y) \leq D_{h\text{-}mean}$ and $D_v(x,y) \leq D_{v\text{-}mean}$. Otherwise N_{cand} is equal to 0.

Finally, the noise decision is: $N(x,y)$ equal to $N_{cand}(x,y)$ if $N_{cand}(x,y) > N_{cand\text{-}mean}$. Otherwise, $N(x,y)$ will be equal to 0, being $N_{cand\text{-}mean}$:

$$N_{cand-mean} = \frac{1}{M \times N} \sum_{x=1}^{M} \sum_{y=1}^{N} N_{cand}(x,y) \quad (10)$$

The noise ratio (*Nr*) to the total number of pixels, where $Noise_{cnt}$ represents the total number of noise pixels is generated by:

$$Nr = \frac{Noise_{cnt}}{M \times N} \quad (11)$$

In this work, the *Br* and *Nr* values were computed, for each band from each image, in five different square areas from our study site, comprising each one about 360000 m^2, and representing the land use of our working area. In this way, two of them, named *U1* and *U2*, were labelled as urban areas. Another two areas (*M1* and *M2*) were listed as mixed areas (urban and agricultural or base soil). The last area (*B*) presented only agricultural and bare soil.

6 PAN Results

For the VHR satellite PAN images tested in this work, the following results can be drawn.

6.1 Histograms of digital numbers

In theory, a number of 2048 (11-bits) possible digital numbers (DNs) values could be collected by both GE1 and WV2 sensors. However, a compression of the range of DNs is done on purpose by the imaging companies to account for extremely reflective surfaces which could create flares [15]. In fact, DN values rarely exceed 1500 in raw VHR satellite imagery without any especial radiometric correction or contrast enhancement. In the case of GE1 imagery, the 99% of the DNs vary between 110 and 780 [16] whereas the main information is distributed between 0 and 10 bits for WV2 imagery [17].

Overall, the peak of the grey level histograms is typically towards the darker values with the right part of the histograms decreasing smoothly and slowly towards the higher DN values [17], [18]. The six DNs histograms (Fig. 2) corresponding to the tested PAN images fit quite well this typical shape. However, a higher compression of the DNs histograms corresponding to the six original PAN VHR satellite images over the whole working area was observed in the WV2 case. This fact can be observed in Fig. 2, where the standard deviations (σ) for the WV2 PAN images turned to be much lower than the attained ones from GE1 PAN images.

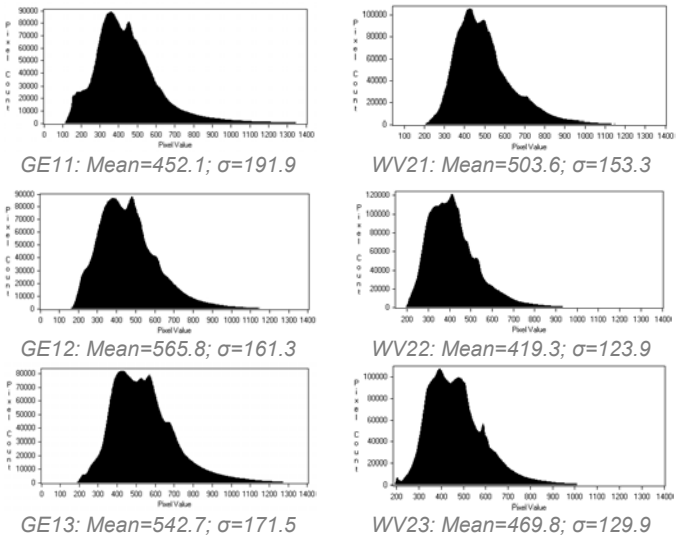

Fig. 2 Histograms and statistics from PAN images over the working area.

6.2 Visual inspection

Fig. 3 is presented to visually illustrate the differences found above between GE1 and WV2 PAN images. Again, clear visual differences between the GE1 PAN images and WV2 ones could be seen, the last appearing blurrier and so showing less contrast. This visual effect can also be appreciated in the second figure of the recent work published by Agugiaro et al. [19] over Trento testfield (Italy).

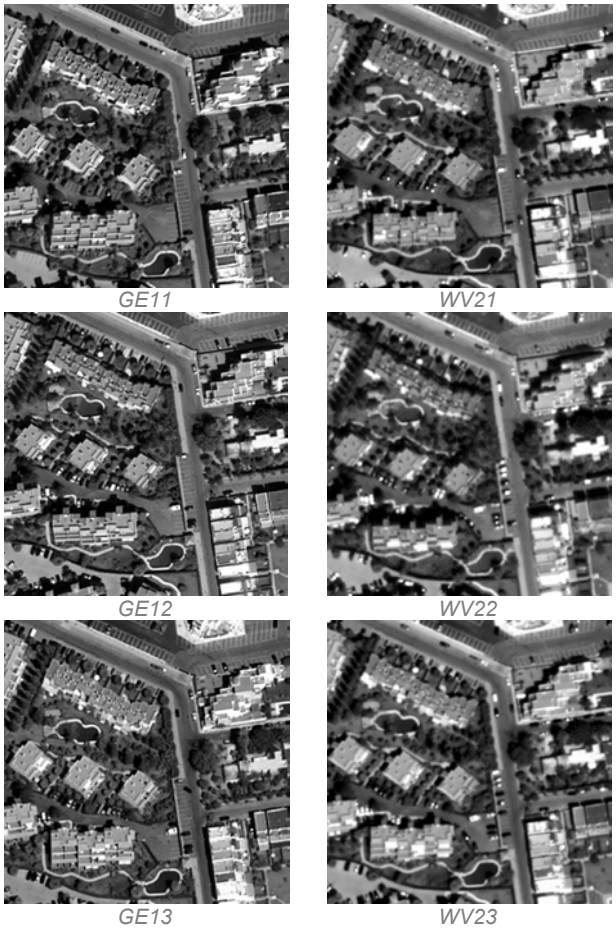

Fig. 3 Visual comparison between the six PAN images over a limited area of 140 m x 140 m.

6.3 Blur and Noise ratios

Tab 3 shows the *Br* and *Nr* indexes computed for the PAN images. Regarding *Br*, GE1 Geo PAN images presented a mean or average value for the five considered of 0.392, 0.389 and 0.496 for GE11, GE12 and GE13 respectively. These general values were much lower than the ones calculated for the WV2 ORS2A images (0.787, 0.919 and 0.902 for WV21, WV22 and WV23). Those differences are quantitatively confirming what can be visually deduced from Fig. 3. Furthermore, for each sensor, the *Br* values were higher with increasing off-nadir angle (which is the complementary angle of the collection elevation angle). In the same way, image blur problem caused by stability incompleteness of the sensor stabilizer has been already reported by [20] working on linear array digital images. This problem was more serious on the forward and backward viewing images than on the nadir viewing image. The behaviour of *Br* with off-nadir and land use is presented in Fig. 4 (for GE1 images) and Fig. 5 (for WV2). It is noteworthy that the differences in *Br* between GE1 and WV2 were much lower on the zone B (bare and agricultural soil without urban areas). In this way, the urban or mixed zones (U1, U2, M1 and M2) presented lower *Br* values for GE1 images, due to the larger content of edges included in them. On the other hand, no significant differences were detected between GE1 images and WV2 ones about *Nr* index.

Image ID	Ratio	Areas					Mean
		U1	U2	M1	M2	B	
GE11	*Br*	0.285	0.322	0.326	0.356	0.670	**0.392**
	Nr	0.377	0.352	0.379	0.360	0.410	**0.376**
GE12	*Br*	0.292	0.265	0.354	0.344	0.690	**0.389**
	Nr	0.375	0.358	0.383	0.365	0.420	**0.380**
GE13	*Br*	0.377	0.391	0.456	0.439	0.816	**0.496**
	Nr	0.371	0.368	0.384	0.363	0.417	**0.381**
WV21	*Br*	0.701	0.777	0.733	0.749	0.976	**0.787**
	Nr	0.381	0.382	0.386	0.390	0.429	**0.394**
WV22	*Br*	0.879	0.922	0.895	0.904	0.996	**0.919**
	Nr	0.384	0.378	0.394	0.384	0.426	**0.393**
WV23	*Br*	0.850	0.909	0.865	0.893	0.995	**0.902**
	Nr	0.379	0.378	0.387	0.364	0.423	**0.386**

Tab. 3 Blur (Br) and Noise (Nr) ratios for each PAN images from GE1 and WV2.

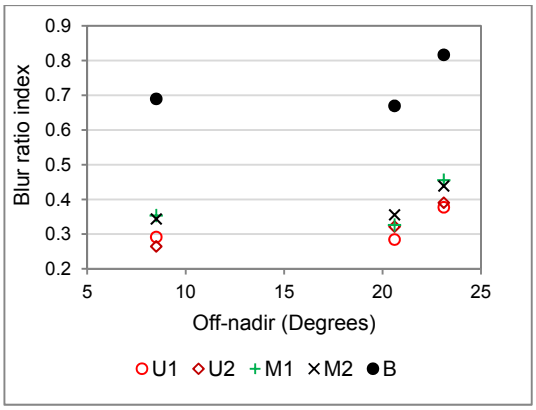

Fig. 4 Blur ratio (Br) behaviour with off-nadir and type of land use for GE1 PAN images.

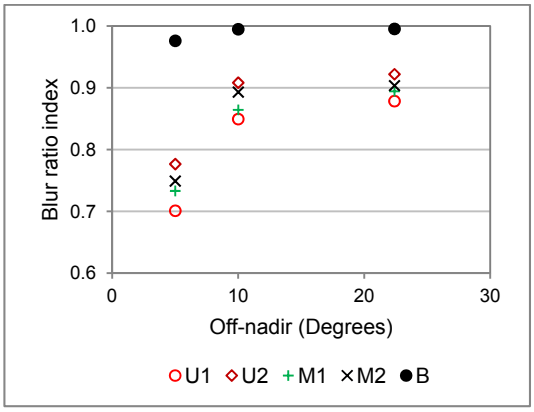

Fig. 5 Blur ratio (Br) behaviour with off-nadir and type of land use for WV2 PAN images.

7 MS Results

Regarding MS images, the results are going to be studied in the three same way used above for PAN images, i.e. histograms of DNs, visual inspection and *Br* and *Nr* indexes.

7.1 Histograms of digital numbers

The histograms computed from each MS band of both MS sensors, in general, presented a similar shape to the PAN images discussed in the last section. Fig. 6 shows the standard deviations (σ) of the histograms for the MS GE1 and WV2 bands in common. As in the case of PAN images, GE1 images presented higher σ values than WV2 for the four classical bands. Moreover, low σ values suggest a higher compression of the DNs histograms. The differences between σ computed for GE1 and the calculated for WV2 ones achieved reached their peak for the Blue band.

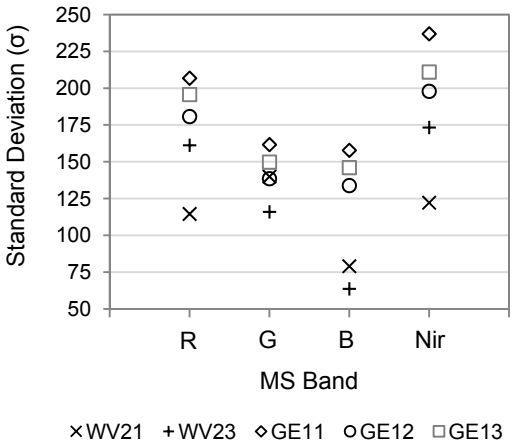

Fig. 6 Standard deviations from the histograms for the bands in common of GE1 MS images and WV2 MS1 ones.

7.2 Visual inspection

Fig. 7 shows a visual inspection of the differences between GE1 and WV2 MS RGB true-colour images. Unlike the PAN images, RGB MS images from GE1 and WV2 did not show any visual and subjective difference. In that sense, the higher GSD for MS images (2 m) could be masked a possible blur effect. Any visual differences were even found when the images with the Blue band were compared.

Fig. 7 Visual comparison between the five MS images (RGB) over a limited area of 140 m x 140 m.

7.3 Blur and Noise ratios

In this section we are going to focus on Br, because any significant difference was detected between GE1 and WV2 MS images about *Nr* index. Thus, Fig. 8 shows the comparison between the *Br* values computed from the four MS classical bands (R, G, B, Nir) included in both sensors, as well as, their relationship with the off-nadir angle. Only three (U2, M1 and B) out of the five areas are presented. Again, the same pattern shown for the PAN images could be seen here. Higher *Br* values are attained with increasing the off-nadir of the image. Also, the MS bands from GE1 images presented *Br* values lower than the MS classical bands from WV2, although the differences were not as higher as for the PAN images. Just as for the PAN images, higher differences were achieved for the urban areas. Regarding the newest WV2's bands, Fig. 9 shows the *Br* computed in U2, M1 and B areas. The Coastal band generated the highest *Br* values for all the land uses tested, presenting lower differences between then. However, the other three bands (i.e. Yellow, Red-Edge and Nir2) showed *Br* quite dependent on the land use.

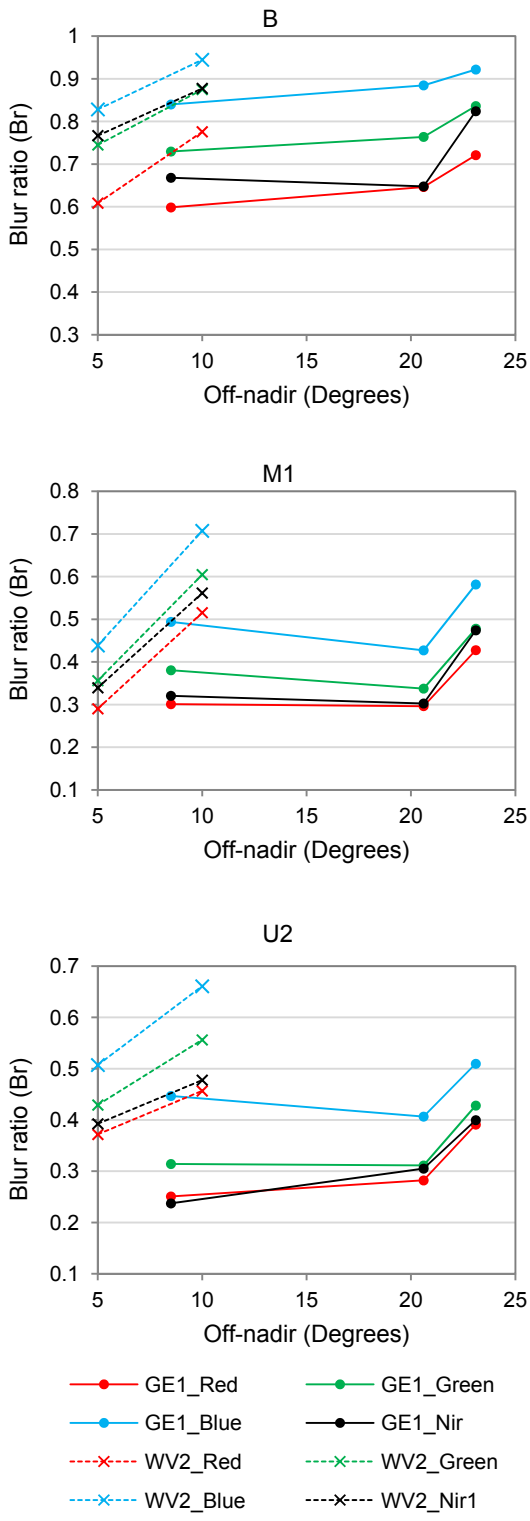

Fig. 8 Blur ratio (Br) behaviour with off-nadir, type of land and band, for the GE1 MS images and WV2 MS1 ones.

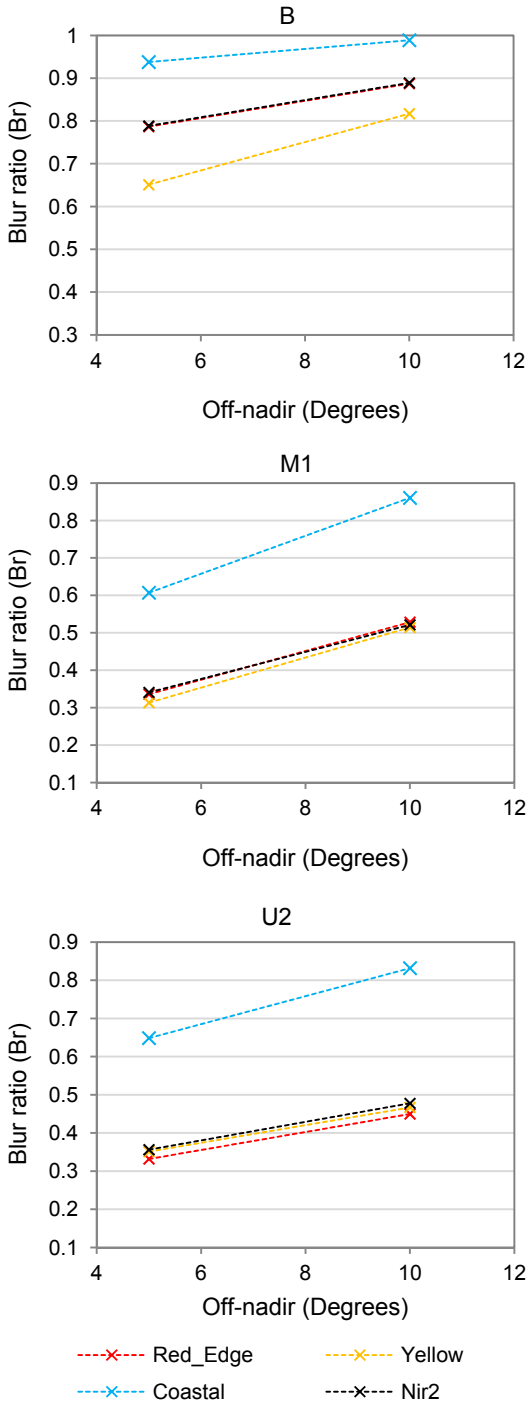

Fig. 9 Blur ratio (Br) behaviour with off-nadir, type of land and band, for the WV2 MS2 images (the newest bands).

8 Discussion

Although the observed lower range of DNs for WV2 ORS2A MS and PAN images might be due to operational aspects of the image acquisition such as sensor viewing angle, sun acquisition angle and atmospheric conditions [16], we hypothesized that the specific radiometric characteristics of both sensor systems and/or the different post-processing applied by the imaging companies could

be behind of this finding. Anyway the results attained in this work should be carefully managed and contrasted to further studies. Thus, it is extremely important to take this research line on to investigate whether the aforementioned radiometric differences between the tested satellite MS sensors can actually affect classification accuracy results. On the other hand, the blur effect of WV2 PAN images could also influence to the matching algorithms for extracting DSM from stereo pairs.

9 Conclusion

The radiometric characteristics and quality based on Digital Numbers (DNs) of several PAN and MS Geo images from GE1 have been compared over the same working area with another Ortho Ready Standard Level-2A (ORS2A) PAN and MS images from WV2.

Radiometric characteristics of the VHR satellite imagery tested in this work, was clearly depending on the off-nadir angle. The higher off-nadir viewing angle, the worse the image quality was. When a comparison were carried out, significant differences in quality and radiometric characteristics between GE1 and WV2 (in both PAN and MS images) were found studying the histograms, by means of visual inspection (mainly in PAN images), and using No-Reference image quality assessment based on Blur and Noise measures. The findings related to the observed lower range of DNs for WV2 ORS2A MS and PAN images, and, the higher *Br* for WV2 images especially for urban and mixed areas, suggest that the quality of the images was worse for WV2 than for GE1. However this fact could be due to operational aspects, further works into the scientific community would be needed for clarify this issue.

Acknowledgement

This work was supported by the Spanish Ministry for Science and Innovation (Spanish Government) and the European Union (FEDER founds) under Grant Reference CTM2010-16573. The authors also appreciate the support from Andalusia Regional Government, Spain, through the Excellence Research Project RNM-3575. Website of the CTM2010-16573 project: http://www.ual.es/Proyectos/GEOEYE1WV2/index.htm.
This work also takes part of the general research lines promoted by the Agrifood Campus of International Excellence ceiA3 as a joint initiative between the universities of Almería, Cádiz, Huelva and Jaén, headed by the University of Córdoba (further information can be retrieved from http://www.ceia3.es/).

References

[1] J. Croft, 2008. *Prodigious Mapping Capabilities, Spatial resolution and Geo-location ability, GeoEye's next-generation Imaging Satellite*. GeoInformatics, 4 (2008) pp 18-23.

[2] R. Pu and S. Landry, 2012. *A comparative analysis of high spatial resolution IKONOS and WorldView-2 imagery for mapping urban tree species.* Remote Sensing of Environment, 124 (2012) pp 516-533.

[3] C.S. Fraser and M. Ravanbakhsh, 2009. *Georeferencing Accuracy of GeoEye-1 Imagery*. Photogrammetric Engineering & Remote Sensing, 75(6) pp 634-638.

[4] M.A. Aguilar, M.M. Saldaña, F.J. Aguilar, I. Fernández, 2012. *Geopositioning accuracy assessment of GeoEye-1 Panchromatic and Multispectral imagery*. Photogrammetric Engineering & Remote Sensing, 78(3) pp 247-257.

[5] M.A. Aguilar, M.M. Saldaña, F.J. Aguilar, 2013. *Assessing geometric accuracy of the orthorectification process from GeoEye-1 and WorldView-2 panchromatic images*. International Journal of Applied Earth Observation and Geoinformation, 21(2013) pp 427-435.

[6] P.J. Åstrand, M. Bongiorni, M. Crespi, F. Fratarcangeli, J. Nowak Da Costa, F. Pieralice, A. Walczyńska, 2012. *The potential of WorldView-2 for ortho-image production within the -Control with Remote Sensing Programme- of the European Commission*. International Journal of Applied Earth Observation and Geoinformation, 19(2012) pp 335-347.

[7] P. Capaldo, M. Crespi, F. Fratarcangeli, A. Nascetti, F. Pieralice, 2012. *DSM generation from high resolution imagery: applications with WorldView-1 and GeoEye-1*. Italian Journal of Remote Sensing, 44(1) pp 41-53.

[8] K. Deilami and M. Hashim, 2011. *Very High Resolution Optical Satellites for DEM Generation: A Review*. European Journal of Scientific Research, 49(4) pp 542-554.

[9] J.K. Liu, J.H. Wu, T.Y. Shih, 2005. *Effects of JPEG2000 on the information and geometry content of aerial photo compression*. Photogrammetric Engineering & Remote Sensing, 71(2) pp 157-167.

[10] T.Y. Shih and J.K. Liu, 2005. *Effects of JPEG 2000 compression on automated DSM extraction: evidence from aerial photographs*. The Photogrammetric Record, 20(112) pp 351- 365.

[11] M.A. Aguilar, M.M. Saldaña, F.J. Aguilar, 2013. *GeoEye-1 and WorldView-2 pan-sharpened imagery for object-based classification in urban environments*. International Journal of Remote Sensing, 34(7) pp 2583-2606.

[12] T. Choi, 2002. *IKONOS Satellite on Orbit Modulation Transfer Function (MTF) Measurement using Edge and Pulse Method*. Master Thesis, South Dakota State University.

[13] M. Crespi and L. De Vendictis, 2009. *A Procedure for High Resolution Satellite Imagery Quality Assessment*. Sensors 9 pp 3289-3313.

[14] M.G. Choi, J.H. Jung, J.W. Jeon, 2009. *No-Reference Image Quality Assessment using Blur and Noise*. International Journal of Electrical and Electronics Engineering, 3(6) pp 318-322.

[15] B. A. McCarty, 2010. *Word of the Month - Bit Depth*. eMap International's GeoViews. Website: http://www.emap-int.com/2010/June/article8.html. Accessed 24 Feb 2013.

[16] M. Crespi, G. Colosimo, L. De Vendictis, F. Fratarcangeli, F. Pieralice, 2010. *GeoEye-1: Analysis of Radiometric and Geometric Capability*. Personal Satellite Services, Second International ICST Conference, PSATS, Rome, Italy, Feb. 2010. Revised Selected Papers, vol. 43, Part 7, pp. 354-369.

[17] D. Poli, E. Angiuli, F. Remondino, 2010. *Radiomeric and geometric analysis of WorldView-2 stereo scenes*. International Archives of the Photogrammetry, Remote Sensing and Spatial Information Science, vol. 38 (Part 1), Calgary, AB, Canada, June 15-18.

[18] E. Baltsavias, M. Pateraki, L. Zhang, 2001. *Radiometric and geometric evaluation of IKONOS Geo images and their use for 3D building modeling*. Proceedings of the ISPRS Workshop "High Resolution Mapping from Space", Hannover, Germany, Sep. 19-21.

[19] G. Agugiaro, D. Poli, F. Remondino, 2012. *Testfield Trento: Geometric evaluation of very high resolution satellite imagery*. International Archives of the Photogrammetry, Remote Sensing and Spatial Information Science, vol. 39 (B8), Melbourne, Australia, 25 Aug.-1 Sep.

[20] L. Zhang, 2005. *Automatic Digital Surface Model (DSM) Generation from Linear Array Images*. Ph. D. Dissertation, no. 88, Institute of Geodesy and Photogrammetry, ETH Zurich, Switzerland.